Flexible and Printed Electronics



# Ultra-sensitive protein detection with organic electrochemical transistors printed on plastic substrate

To cite this article before publication: Eleonora Macchia *et al* 2018 *Flex. Print. Electron.* in press https://doi.org/10.1088/2058-8585/aad0cb

# Ultra-Sensitive Protein Detection with Organic Electrochemical Transistors Printed on Plastic Substrate

Eleonora Macchia[1], Paolo Romele[2], Kyriaki Manoli[1], Matteo Ghittorelli[2], Maria Magliulo[1], Zsolt M. Kovács-Vajna[2], Fabrizio Torricelli[2,#], Luisa Torsi[1,3,#]

[1] Department of Chemistry, University of Bari, Bari 70126, Italy

[2] Department of Information Engineering, University of Brescia, Brescia 25123, Italy

[3] The Faculty of Science and Engineering, Åbo Akademi University, Turku, Finland

[#] Corresponding authors: fabrizio.torricelli@unibs.it and luisa.torsi@uniba.it

***Abstract*:** The detection of protein biomarkers is of great importance in the early diagnosis of severe pathological states. Although in the last decade many approaches to achieve ultra-sensitive protein detection have been developed, most of them require complicated assay set-ups, hindering their adoption in point-of-care applications and on-spot diagnosis. Here we show an organic electrochemical transistor (OECT) biosensor printed on plastic substrates that can selectively detect Immunoglobulin G (IgG) with unprecedented attomolar detection limit. The OECT is used as a transducer of the biorecognition event taking place at the gate electrode. The measured concentrations are well below the detectable limits of the leading clinical diagnostic ELISA assay, and comparable to the ones gathered with the label-needing single molecule arrays (SiMoA) platform. Our work benchmarks the role of plastic OECT-based biosensors as a powerful tool in simple, low-cost, yet non-invasive, ultra-sensitive, and widely applicable immunoassay technology.

***Keywords*:** OECTs, Protein Detection, Plastic Biosensors, Immunosensors

## *1. Introduction*

The US National Institute of Health defines biomarkers as "molecules that can be objectively measured and evaluated as indicators of normal or disease processes and pharmacologic responses to therapeutic intervention" [1]. Consequently, an area of intense investigation has risen from the excellent clinical and preclinical applications of these molecules. Among the plethora of biomarkers able to distinguish between two or more biological states, the sensitive detection of proteins is of paramount importance in a number of clinical fields, such as oncology [2], neurology [3], inflammation [4] and infectious diseases [5]. The clinical use of protein biomarkers as indicators of the onset, existence or progression of pathological states, requires the measurement of low concentrations of proteins in complex samples. In fact, the serum concentrations of the majority of protein biomarkers of cancer, neurological disorders and infections at the early stages range from $10^{-18}$ M to $10^{-15}$ M [5]. So far, enzyme-linked immunosorbent assays (ELISAs) have served as the gold-standard in high throughput clinical protein determinations. However, due to the lack of high sensitivity (detection in the picomolar, $10^{-12}$ ·mole $L^{-1}$, pM range) [6], ELISA is not able to detect clinically relevant biomarkers in serum at ultra-low detection limit. Therefore, attempts to develop ultra-sensitive assays for the detection of various protein biomarkers have been done by several groups in the last few years. Notable works have utilized electrochemical microfluidic arrays [7], electrochemical immunosensors with gold nanoparticles functionalized with magnetic multi-walled carbon nanotubes [8] and novel laser-induced fluorescence systems [9]. Although these reports advanced the field of ultra-sensitive biomarker detection, they require complicated assay set-ups, time consuming sample preparation and are potentially subject to sensor fouling. Recently, a method based on counting single labelled immunocomplexes captured on paramagnetic beads in single molecule arrays (SiMoA) has been proposed [10]. Interestingly, the SiMoA assay has enabled detection of prostate specific antigen (PSA) in the attomolar (aM, $10^{-18}$ M) range [11]. However, SiMoA is a label-needing technique as the ultra-sensitive detection requires highly fluorescent species that need to be chemically conjugated to one of the reaction partners [12] and suffers in limitations of the analysis time and equipment costs. Besides, the complexity of the SiMoA detecting apparatus is not compatible with Point-of-Care (POC) applications. In fact, the ultimate goal in early diagnosis of severe pathological states is the development of highly accurate and cheap POC disposable devices, simple enough to be used at the primary care level, in remote and low resource settings with no laboratory infrastructure. Therefore, POC has the potential to improve the management of diseases as well as of regular medical check-up testing [13]. In this perspective, printable and flexible organic bioelectronics represents a powerful tool for ultra-sensitive detection of protein biomarkers in clinical settings. As far as the biosensors are concerned,

the quality of the analytical electronic response and the ultralow detection limits foreseen will offer the possibility of performing reliable quantitative assays of proteins in biological fluids such as blood, saliva and tears. Eventually, a label free non-invasive strip test can be envisaged based on bioelectronic sensors printed at low cost on plastic or even paper substrates [14]. Several research groups have contributed to the advancement in the field of printed bioelectronics, integrating a biological recognition layer into novel structures based on organic thin film transistors (OTFTs), such as organic electrochemical transistors (OECTs) and organic field effect transistors (OFETs) [15,16,17,18]. Besides, OECTs are particularly suitable for biosensing applications because the devices can stably operate in aqueous environment, such as blood serum, saliva or tears. An OECT consists of an ion permeable organic semiconductor (OSC), in contact with an electrolyte. The gate electrode is immersed in the electrolyte solution that acts as the solid-state gate insulator in standard FETs, while source and drain electrodes establish contact with the OSC. Being made with ion permeable OSCs, the OECT operation relies on the ion exchange between the electrolyte solution and the OSC [19,20]. OECTs can be made with both p-type and n-type materials [21]. In particular, in the case of a p-type OECTs when a positive voltage is applied to the gate electrode ($V_G$) cations are injected in the OSC. The injected cations de-dope the OSC that decreases its conductivity. On the other hand, when a negative voltage is applied to the gate electrode anions are injected in the OSC. The injected anions dope the OSC that increases its conductivity. In the OECT the electronic charge carriers drift under the source-drain voltage ($V_D$). Therefore, the resultant source-drain current ($I_D$) is proportional to the quantity of mobile holes or electrons in the OSC and hence probes the doping state of the OSC.

A typical material for OECTs is the conducting polymer poly(3,4-ethylenedioxythiophene) doped with poly(styrenesulphonate) (PEDOT:PSS) [22,23]. This material has attracted interest for its high hole conductivity (>1000 S $cm^{-1}$), high stability and for its commercial availability as an aqueous dispersion for solution processing. The semiconducting polymer PEDOT is p-type doped by the PSS, since the sulphonate anions of PSS are compensated by mobile holes in PEDOT. To the best of our knowledge Matsue et al. [24] were the first to incorporate a bio-recognition element into an OECT and thereby achieve a chemically selective biosensor with an organic transistor as the transducer (often called a micro-electrochemical enzyme transistor or enzyme switch, whenever the bio-recognition element is an enzyme). Malliaras and his team, demonstrated a cascade of PEDOT:PSS-based sensor transistors for different bioelectronic applications [25,26], showing a detection limit of glucose of 100 mM [27]. OECT based biosensing platforms have been proposed as immunosensors, as well. Using goat anti-rabbit IgG, detection of rabbit IgG at the nanomolar ($10^{-9}$ M, nM) limit has been shown [28]. Kim et al. demonstrated a functionalized OECT

immunosensor to detect prostate specific antigen / a1-antichymotrypsin complex with a limit of detection of about 100 fM [29]. Recently, the gold gate electrode of an OECT device has been modified with a specific human epidermal growth factor receptor 2 (HER2) antibody to capture HER2 proteins in solutions [30]. The device has been proved to detect HER2 down to the level of 10 $10^{-15}$ M. Our group has recently proven that anti-human Immunoglobulin G (anti-IgG) antibodies immobilized on the gate electrode surface of an OECT can reliably detect IgG affinity ligands down to a nominal concentration of 6 $10^{-15}$ M [22]. Here, we present a flexible and printed PEDOT:PSS OECT-based immunosensor for detection of Immunoglobulin G (IgG) at the atto-molar detection limit. The anti-IgG is employed as capturing protein to ensure that only its affinity ligand, i.e. the IgG, is selectively detected. A negative control experiment with bovine serum albumin (BSA) immobilized on the gate electrode surface instead of anti-IgG has been designed to assess that the IgG-induced electronic response is actually due to the sole antigen-antibody complex formation. Moreover, the OECT response to the IgG antigen is rationalized through physical modelling of the measured electrical characteristics. The OECT-based immunosensor enables at the same time an ultra-low limit of detection and selectivity. The further improvement achieved in the limit of detection represents a breakthrough in label-free assay. Indeed, to the best of our knowledge, a detection limit comparable to the one obtained with SiMoA platforms has been accomplished for the first time with a flexible and printed OECT relying on a label free immunoassay. Hence, the proposed platform opens up new relevant opportunities in the field of printed and low-cost array platforms for point-of-care early-diagnosis with a foreseen huge impact of a simple and widely applicable ultra-sensitive immunoassay technology.

## *2. Methods*

### *2.1 Materials*

Polyethylene substrates, dimethyl sulfoxide (DMSO), anti-human IgG, IgG, bovine serum albumin (BSA), ethanolamine, 1-Ethyl-3-(3-dimethylaminopropyl)-carbodiimide (EDC), N-Hydroxysulfosuccinimide sodium salt (Sulfo-NHS), water for high performance liquid chromatography (HPLC-grade), and phosphate buffered saline (PBS) tablets were purchased by Sigma-Aldrich. Anti-Human IgG, IgG and BSA are used with no further purification. Each tablet dissolved in 200 mL of deionized water yields 0.01 M phosphate buffer, 0.0027 M potassium chloride and 0.137 M sodium chloride, pH 7.4 at 25 °C. PEDOT:PSS PH-500 in aqueous dispersion was purchased by Heraeus Clevios GmbH.

*2.2 OECTs Fabrication*

The polyethylene foils were cleaned in a deionized water ultrasonic bath for 15 min at room temperature. After the cleaning, the substrates were treated using oxygen plasma. Gold source and drain contacts were evaporated through a shadow mask. The gold thickness was about 100 nm. The PEDOT:PSS was deposited by using a desktop printer Epson L-300 with a printing resolution of 5760 x 1440 dpi and a minimum droplet size of 3 pl. A thermal treatment at 50 °C for 60 s in oven was performed between each printing step. The total PEDOT:PSS thickness amounted to t = 450 nm and was obtained by printing 8 layers. The device width and length were W = 1200 μm and L = 120 μm, respectively. The samples were eventually annealed in oven at 90 °C for 10 min. A polydimethylsiloxane well was glued around the channel area and filled with 300 μl of PBS ($10^{-2}$ M) acting as gating medium.

*2.3 Gate Electrode Functionalization*

A Kapton® foil (area of ~ 0.6 $cm^2$) covered by e-beam evaporated gold (50 nm) on titanium (5 nm) served as the gate electrode. The gate electrodes were cleaned in an ultrasonic bath of isopropanol for 10 minutes and treated for 10 min in ozone cleaner. The Self Assembled Monolayer (SAM) functionalization protocol involves a mixed alkanethiol SAM strategy, prepared in ethanol (puriss p.a. grade). The gold electrodes were immersed into the mixed SAM solution and kept in the dark under $N_2$ for 18 h at 22 °C. The SAMs were then activated by immersion into a water solution of 0.2 M EDC (1-Ethyl-3-(3-dimethylaminopropyl)-carbodiimide) and 0.05 M Sulfo-NHS (N-Hydroxysulfosuccinimide sodium salt) for 2 h at 25 °C. Anti-IgG or BSA (100 μg/mL) in Phosphate Buffer Solution (PBS, pH = 7.4) was left to immobilize for 2 h at 25 °C. To prevent non-specific adsorption ethanolamine (1M) in PBS solution was left to immobilize for 1 h at 25 °C [31]. The functionalized gate electrode was then stably immersed into the PBS on top of the well as schematically depicted in Fig. 1a.

*2.4 Measurement of the OECT I-V Curves*

The electrical characteristics were measured with an Agilent 4155C semiconductor parameter analyzer at room temperature (21 °C) in air. Both output and transfer characteristics were measured using 10 mM PBS as electrolyte. Output characteristics were measured by sweeping the drain voltage ($V_D$) and recording the drain current ($I_D$) at several gate voltages ($V_G$). The drain voltage was swept from 0 V to -0.8 V. In the case of the transfer characteristics, $I_D$ was measured as a

function of $V_G$ ranging from 0.3 V to -0.8 V at $V_D$ = -0.4 V. All the applied voltages were referred to the source contact. The functionalized gate electrode was then incubated (at room temperature and in the dark) for 10 min in 100 µl of PBS. The gate electrode was removed from the PBS solution, washed thoroughly water to remove the unbounded IgG and immersed into the electrolyte in front of the PEDOT:PSS channel as schematically depicted in Fig. 1a. The transfer characteristic was then recorded and the current at the maximum transconductance is addressed as the "$I_0$" current base-line. After the measurement of the $I_0$ base-line, the same functionalized gate electrode was incubated (at room temperature and in the dark) for 10 min in 100 µl of the PBS standard-solutions of the ligands (IgG) with nominal concentrations ranging from 6 aM to 60 pM. After incubation in each PBS standard-solution of IgG starting from the more diluted one, the functionalized gate electrode was washed thoroughly to remove the unreacted ligands away. The $I_D$-$V_G$ transfer curve was then measured, and the current at the maximum transconductance is addressed as the "I" signal at a given concentration.

## *3. Results and Discussion*

### *3.1 Measurement of the Immunosensor Calibration Curve*

Fig. 1a shows the OECT schematic structure. The device channel is made of PEDOT:PSS printed on a flexible plastic substrate and contacted by means of the source and drain gold electrodes. The gate electrode consists of a gold plated Kapton foil functionalized with a very compact self-assembled monolayer (SAM) of the capturing Anti-IgGs, schematically shown in Fig. 1b. A PDMS well confines 300 µl of 10 mM PBS on the channel area that establishes the ionic connection between the gate electrode and the PEDOT:PSS channel.

All the data discussed from here on were gathered on OECTs appropriately cycled to reach the operational stability, being the stability of the transistor under operation. All the reported devices had to be stabilized before reaching a stable operation, by repeated cycling of the transfer curve until overlap of at least three subsequent traces was obtained. The cycling was performed rigorously in the gate voltage range that minimized any electrochemical process, which minimized the gate leakage currents. Fig. 2a and 2b show the transfer characteristics measured with anti-IgG and BSA gate electrodes, respectively. $I_D$ was measured as a function of $V_G$ (ranging from 0.3 V to -0.8 V) with a fixed drain voltage of -0.4 V. The characteristics show that at positive gate voltages cations penetrate the PEDOT:PSS film and de-dope the semiconductor, resulting in a drain current of the order of 10 µA. On the other hand, at negative gate voltages anions are injected in the

semiconductor, increasing its conductivity and resulting in a current of the order of mA. The insets of Fig. 2a and 2b show the corresponding transconductance $g_m = \delta I_D/\delta V_G$ using anti-IgG and BSA gates, respectively. The maximum measured transconductance is of the order of the mS, which is in agreement with state of art OECTs [32, 33]. Typical OECT output characteristics measured with anti-IgG and BSA functionalized gate electrode s are displayed in Fig. 2c and 2d, respectively. The drain is swept from 0 V to -0.8 V, while $V_G$ ranges from 0.2 V to -0.6 V with a -0.2 V voltage step. The output characteristics show a clear transition from a linear regime to a saturation regime, with an almost flat saturation current (Fig. 2c and 2d). The electrical characteristics exhibit the hallmark of OECTs, that is the low voltage operation in the stability window of water ($|V| \leq 1$ V). Another quite relevant aspect is that the device herein presented does not require the use of the reference electrode. In fact, the OECT gate should be an ideally polarizable electrode. In order to fulfill this assumption, the potential window for $V_G$ has been chosen so as to avoid any electrochemical process. Also relevant is that in such a configuration the presence of a reference electrode as gate, could be even detrimental as the faradaic current in the electrode systematically depolarizes the charge double layer, thus cancelling the effect of the capacitive coupling between the bio-layer and the electronic channel. In fact, the IgG detection is performed by measuring the OECT transfer characteristics after incubation of the anti-IgG functionalized gate electrode in 100 μl of PBS standard solutions of IgG ranging from 6 aM to 60 pM nominal concentrations. The PBS solution reproduces a physiologically relevant environment having a pH of 7.4 and an ionic-strength of 162 mM. Fig. 3a shows typical sensing transfer characteristics, measured after incubation of the same anti-IgG functionalized gateelectrode into progressively more concentrated IgG standard-solutions. The black-curve, taken as the base-line, is measured after incubation of the functionalized gateelectrode in bare PBS solution. The subsequently measured grey-curve corresponds to the incubation in the 6 aM IgG solution. The black and grey curves are significantly different. This trend is reproduced as the standard-solutions at increased IgG concentration are progressively assayed assessing a biosensor's dynamic range of up to eight orders of magnitude. As shown in the inset of Fig. 3(a), a first anti-IgG functionalized gate is used for the IgG sensing measurements, while, after the assay, a switching of the gate electrode to a second non exposed anti-IgG one is performed. The transfer curves measured before and after the exposure to IgG, represented as the black and the light blue curves in the inset of Fig. 3(a), showed a relative current change of -2.8%. This control experiment allows to assess that only the dose curves that involve a minor $I_{DS}$ current decreases (presumably due to a slight degradation of the transport properties of the organic semiconductor) are acceptable. Such a procedure rules out that the current changes measured during the sensing experiments could be attributed to a device performance degradation.

The OECT responses (relative current variations) to IgGs in PBS standard-solutions are shown in Fig. 3b as black circles, while the red circles are the responses to IgG assayed with a BSA functionalized gateelectrode. The response is directly evaluated from the measured transfer characteristics and reads:

$$\frac{\Delta I}{I_0} = \frac{I - I_0}{I_0} \quad (1)$$

Where $I$ is the drain current measured after incubation with the target IgG concentration and and $I_0$ is the baseline drain current.

Fig 3b(black circles) showsthe average and standard deviation of $\Delta I/I_0$ over three replicates. The sensor response is 9% at the minimum IgG concentration (6 aM), it monotonically increases of about 3%/dec with a maximum response equal to 23% at 60 pM. The sensor response cover a concentration range of eight orders of magnitude. The level of response is in agreement with state-of-art label-free FET biosensors [34,35,36,37]. In addition, we note that possible routes for enhancing the sensor response could be the further optimization of the functionalization protocol of the gate electrode and/or the use of advanced OECT-based configurations [38]. As a control experiment, Fig. 3b (red squares) shows the responses to IgG assayed with a BSA functionalized gate electrode. Importantly, the negative-blank control confirms that no significant response to IgG exposure is measured when a gold gate electrode functionalized with BSA is used. In fact, the high selectivity of the OECT biosensing platform is effectively proven by the almost zero response of the control assay in the whole concentration range.The limit of detection (LOD) has been computed, being the concentration that leads to a response of $(\Delta I/I_0)_{mean} \pm k\sigma$, where $(\Delta I/I_0)_{mean}$ is the average response of the blank sample, $\sigma$is the relative standard deviation and k is a numerical factor chosen according to the level of confidence required. IUPAC recommends a value of k = 3 as the probability of a blank signal being 3-fold higher than the $(\Delta I/I_0)_{mean}$(*i.e.* a false positive) is less than 1%. According to this definition, a LOD level of 8% is estimated from the noise level of the control experiment. The OECT response at 6 aM is beyond the LOD and prove that the OECT assay is capable to reach the sensitivity of the SiMoA platform with a much simpler apparatus. As a further confirmation, a control experiment is designed in order to rule out that the reported variation could be due to a degradation of the biosensor. To this aim, two gate electrodes functionalized with anti-IgG are fabricated at the same time and in the very same experimental conditions. One gate is used for the IgG sensing measurements and the transfer characteristics as a function of the IgG concentration are recoded. Then, after performing the assay, a transfer characteristic is measured

with the other (pristine) gate. The inset of Fig. 3a shows a comparison between the transfer characteristic obtained with the first gate electrode before the biosensing and with the second (pristine) gate electrode, which has not been incubated with IgG (the same OECT is used in both cases). The two transfer characteristics are almost perfectly overlapped when $V_G$> -0.6 V while the current measured with the pristine gate electrode is slightly lower when $V_G$< -0.6 V. This control experiment shows a maximum relative current variation equal to 2.8%, which is in agreement with the BSA control experiments shown in Fig. 3b (red symbols). It is worth noting that the control experiment accounts for both the degradation of the organic semiconductor after the sensing of eight IgG concentrations and the variability due to the fabrication process of the gate electrodes.

*3.2 Modeling of the Immunosensor Electrical Characteristics*

To gain physical insight on the immunosensor response, the transfer characteristics of the anti-IgG functionalized OECT as a function of the IgG concentrations have been reproduced with the state of art model firstly introduced by Bernards and Malliaras [39]. The model reads [40,41]:

$$I_D = -\frac{G}{2V_p}\left(V_p - V_e\right)^2 \text{ if } V_D < V_e - V_p \tag{2}$$

$$I_D = -\frac{G}{V_p}\left(V_p - V_e + \frac{V_D}{2}\right) \text{ if } V_D \geq V_e - V_p \tag{3}$$

where

$$G = \frac{Wt}{L} q\mu p_0 \tag{4}$$

$$V_p = \frac{q p_0 v}{C} \tag{5}$$

$$V_e = V_G \frac{C}{C_p} + V_o \tag{6}$$

$$C = \left(\frac{C_g C_p}{C_g + C_p}\right) \tag{7}$$

where W, t, L are the width, thickness and length of the semiconducting channel, respectively. q is the elementary charge, $\mu$ = 2 $cm^2/Vs$ is the hole mobility [42], $p_0$ = 1.8 $10^{20}$ $cm^{-3}$ is the intrinsic doping of the organic semiconductor [39], and v = W t L is the volume of the PEDOT:PSS. C is the overall capacitance, which accounts for the series of the electric-double-layer capacitance at the gate-electrolyte interface ($C_g$) and the PEDOT:PSS capacitance ($C_p$= $C_v$ v), where $C_v$ = 40 F / $cm^3$ is the volumetric capacitance [42] and hence $C_p$ = 2.6 µF. $V_e$ is the electrolyte voltage, $V_G$ is the voltage applied to the gate electrode and $V_o$ is the potential drop at the gate-electrolyte interface and it accounts for the variation of the net charge and/or dipole moment at the bio-functionalized gate electrode due to the binding events. These charge-mediated variations results in a variation of the

work function of the gate electrode and are widely reported in the case of electrolyte-gate FETs with bio-functionalized gate [16, 43]. G is the OECT conductance that depends only on geometrical and physical parameters (Eq. 4) and $V_p$ is the pinch-off voltage. It is worth noting that the presented model has two parameters, namely $C_g$ and $V_o$, which could be affected by the bio-recognition event taking place on the biofunctionalized gate electrode. Since the biorecognition event results in a variation of the electrolyte potential $V_e$ through the change of both $C_g$ and $V_o$ (Eqs. 6, 7), we used a reference-less device configuration. This configuration allows the measurement of the electrical variations taking place at the gate electrode provided the suitable design of the gate and channel geometries. It is worth noting that when the biorecognition events occur at the semiconductor interface (i.e. the semiconductor is biofunctionalized) a reference-electrode device configuration could be used. This simplifies the measurement setup but does not enable the measurement of the capacitance variation.

[R1.4] In order to be maximize the sensitivity to the variations of $C_g$, the immunosensor has to be designed with a suitable ratio between the gate capacitance $C_g$ and the PEDOT:PSS capacitance $C_p$. More in detail, Eq. 7 shows that in the case $C_g \gg C_p$, results $C \cong C_p$ and therefore the biosensor is insensitive to variations of $C_g$. On the other hand, in the case $C_g \ll C_p$, $C \cong C_g$, $V_e$ weakly depends on $C_g$ and, in turn, on $V_G$ (Eq. 6) thus yielding a reduced sensitivity and hindering the low-voltage operation. Since the gate and the PEDOT:PSS capacitances depend on the gate electrode area and the PEDOT:PSS volume, respectively, it follows that a balanced tuning of the gate electrode and the PEDOT:PSS geometries is paramount in order to guarantee both sensitivity to variations of $C_g$ and low-voltage operation. To this aim, we found that $C_g \cong 5\,C_p$ optimizes both the aforementioned conditions enabling the biosensor operation in the IgG concentration range $6\ 10^{-18}$ M - $6\ 10^{-11}$ M.

We systematically reproduced the measured transfer characteristics as a function of the ligand concentration (Fig. 3a) by means of the OECT model. The slope of the drain current yields $V_p$, and in turn C (Eq. 5), while the voltage shift yields $V_o$. Therefore, the two physical parameters can be independently extracted from different and well-defined regions of the transfer characteristic. The extracted parameters as a function of the ligand concentration are shown in Fig. 4. More in detail, the inset of Fig. 4a shows $V_p$ as a function of the IgG concentration. The sensitivity of $V_p$ is about 6.2 mV/dec. In the case of the first incubation at 6 aM of IgG, the variation from the baseline is 10.8 mV. It is worth to note that a variation of $V_p = (qp_0v)/C$ is due to the variation of the electric double layer capacitance at the gate-electrolyte interface $C_g$ where the binding event takes place. The variation of $C_g$ can be ascribed to the antigen-antibody binding that lowers the dielectric constant of the biolayers and results in a reduced overall capacitance per unit area [15]. Fig. 4a

shows the extracted gate capacitance $C_g$ as a function of the IgG concentration. $C_g$ amounts to 13.5 μF (baseline) and decreases of about 1 μF after the first incubation at 6 aM of IgG. Further increasing the IgG concentration leads to a $C_g$ decrease of about 0.4 μF/dec. Fig. 4b shows $V_o$ as a function of the IgG concentration. After an initial variation of about 56 mV after the exposure to 6 aM of IgG, $V_o$ decreases of about 10 mV/dec. The decreasing of $V_o$ after the binding of anti-IgG and IgG molecules can be attributed to an increase of the positive charges and/or dipole moment at the functionalized gate electrode that results in a larger $V_e$ for the same applied $V_g$. This is in agreement with electrolyte-gated FETs [43] and with more specific functional bio-interlayer structures [16] used to evaluate the protein interactions. As a result, the combined variation of both $C_g$ and $V_o$ leads to the unprecedented sensitivity of the proposed device to the detection of proteins.

### *4. Conclusions*

In summary, OECTs operated with a gate electrode modified with anti-human Immunoglobulin G antibodies have been successfully used for the detection of human Immunoglobulin G (IgG) down to the attomolar limit. The detection limit is several orders of magnitude lower than those of conventional electrochemical approaches. Interestingly, the OECT assay can reach the sensitivity of the SiMoA platform with a simpler apparatus. The outstanding sensitivity lies in the transistor structure, which amplifies the combined effects of variation of the gate electrode capacitance and work function after a detection event has occurred. Both the OECTs and the biofunctionalized gate electrode are deposited on plastic foil resulting in an ultra-low cost high-performance technology for the widespread application of ultra-sensitive biosensors. Moreover, given the general approach engaged in the gate electrode functionalization procedure, the platform is in principle applicable for the detection of a wide spectrum of clinically relevant biomarkers. Therefore, this work shows significant promises for the use of OECTs in the field of early on-the-spot diagnosis as non-invasive, ultra-sensitive approach, assessing progress toward point-of care applications.

### *Acknowledgments*

"OrgBIO" Organic Bioelectronics (PITN-GA-2013-607896), "Sense-of-Care" OFET biosensors for point-of-care applications (PITN-2012-GA-316845) projects.

***References***

[1] Manne U., Srivastava R.G., Srivastava S., **2005**, *Drug Discovery Today*, 10, 965-976.
[2] Rusling J.F., Kumar C.V., Gutkind J.S., Patel V., **2010**, *Analyst*, 135, 2496-2511.
[3] Shaw L.M. *et al.*, **2009**, *Ann. Neurol*., 65, 403-413.
[4] Toedter G., Hayden K., Wagner C., Brodmerkel C., **2008**, *Clin. Vaccine Immunol*., 15, 42-48.
[5] Barletta J.M., Edelman D.C., Constantine N.C., **2004**, *Am. J. Clin. Pathol.*, 122, 20-27.
[6] Lilja H., Ulmert D., Vickers A.J., **2008**, *Nat. Rev. Cancer*, 8, 268-278.
[7] Malhotra R. *et al*., **2012**, *Anal. Chem*., 84, 6249-6255.
[8] Li F., Han J., Jiang L., Wang Y., Li Y., Dong Y., Wei Q., **2015**, *Biosensors and Bioelectronics*, 68, 626-632.
[9] Zhang J., Wang S., Liu K., Wei Y., Wang X., Duan Y., **2015**, *Anal. Chem*. 87, 2959-2956.
[10] Chang L., Rissin D.M., Fournier D.R., Piech T., Patel P.P., Wilson D.H., Duffy D.C., **2012**, *J. Immunol. Methods*, 378, 102-115.
[11] Schubert S.M., Arendt L.M., Zhou W., Baig S., Walter S.R., Buchsbaum R.J., Kuperwasser C., Walt D.R., **2015**, *Scientific Reports*, 5, 11034.
[12] Rissin D.M. *et al*., **2010**, *Nat. Biotechnology*, 28(6), 595-599.
[13] Torsi L., Magliulo M., Manoli K., Palazzo G., **2013**, *Chem. Soc. Rev*., 42, 8612-8628.
[14] Manoli K., Magliulo M., Mulla M.Y., Singh M., Sabbatini L., Palazzo G., Torsi L., **2015**, *Angew. Chem. Int. Ed*., 54, 12562-12576.
[15] Mulla M.Y., Tuccori E., Magliulo M., Lattanzi G., Palazzo G., Persaud K., Torsi L., **2015**, *Nat. Commun.*, 6, 6010.
[16] Macchia E., Alberga D., Manoli K., Mangiatordi G.F., Magliulo M., Palazzo G., Giordano F., Lattanzi G., Torsi L. **2016**, *Scientific Reports*, 6, 28085.
[17] Demelas M., Lai S., Spanu A., Martinoia S., Cosseddu P., Barbaro M., Bonfiglio A., **2013**, *J. Mater. Chem B*, 1, 3811-3819.
[18] Spijkman M.J., Brondijk J.J., Geuns T.C., Smits E.C., Cramer T., Zerbetto F., Stoliar P., Biscarini F., Bloom P.W., de Leuw D.M., **2010**, *Adv. Funct. Mater*., 20, 890-905.
[19] Rinay J., Inal S., Salleo A., Owens R.M., Berggren M., Malliaras G.G., **2018**, *Nat. Mater. Review*, 3, 17086.
[20] Kim S.H., Hong K., Xie W., Lee K.H., Zhang S., Lodge T.P., Frisbie C.D., **2013**, *Adv. Mater*., 25, 1822–1846
[21]Giovannitti A. *et al*., **2016**, *Nat. Commun*., 7, 13066.
[22] Macchia E., Ghittorelli M., Torricelli F., Torsi L., **2017**, Advances in Sensors and Interfaces (IWASI), 7th IEEE International Workshop, 68-72.
[23] Rivnay J., Inal S., Collins B.A., Sessolo M., Stavrinidou E., Strakosas X., Tassone C., Delonchamp D.M., Malliaras G.G.,**2015**, *Nat. Commun.*, 7, 11287.
[24] Matsue T., Nishizawa M., Sawaguchi T., Uchida I., **1991**,*J. Chem.Soc. Chem. Commun*.,1029–1031.
[25] Berggren M., Richter-Dahlfors A., **2007**, *Adv. Mater*., 19, 3201–3213.
[26] Mabeck J.T., Malliaras G.G., **2006**, *Anal. Bioanal. Chem*., 384, 343–353.
[27] Zhu Z.T., Mabeck J.T., Zhu C., Cady N.C., Batt C.A., MalliarasG.G.,**2004**, *Chem. Commun.*, 7, 1556.
[28] Kanungo M., Srivastava D.N., Kumar A., Comtractor A., **2002**, *Chem. Commun*., 7, 680.
[29] Kim D.J., Lee N.E., Park J.S., Park I.J., kim J.G., Cho H.J., **2010**, *Biosens. Bioelectron*., 25, 2477.
[30] Fu Y., Wang N., Yang A., Law H.K., Li L., Yan F., **2017**, *Adv. Mater*., 1703787, 1-7.
[31] Holzer B., Manoli K., Ditaranto N., Macchia E., Tiwari A., Di Franco C., Scamarcio G., Palazzo G., Torsi L., **2017**, *Adv. Biosys*., 1700055, 1-10.
[32] Rivnay J., Leleux P., Sessolo M., Khodagholy D., Hervé T., Fiocchi M., Malliaras G.G., **2013**, *Adv. Mater*., 25,7010-7014.

[33] Khodagholy D., Rivnay J., Sessolo M., Gurfinkel M., Leleux P., Jimison L.H., Stavrinidou E., Herve T., Sanaur S., Owens R.M., Malliaras G.G., **2013**, *Nat. Commun.*, 4, 2133.
[34] Palazzo G., De Tullio D., Magliulo M., Mallardi A., Intranuovo F., Mulla M.Y., Favia P., Lundin I.V., Torsi L., **2015**, *Adv. Mater.*, 27, 911-916.
[35] Ishikawa F.N., Curreli M., Chang H.K, Chen P.C., Zhang R., Cote R.J., Thompson M.E., Zhou C., 2009, ACS Nano, 12, 3969-3976.
[36] Hammock M.L., Knopfmacher O., Naab B.D., Tok J.B.H., Bao Z., **2013**, *ACS Nano*, 7, 3970-3980.
[37]Gualandi I., Marzocchi M., Scavetta E., Calienni M., Bonfiglio A., Fraboni B., **2015**, *J. Mater. Chem. B*, 3, 6753-6762.
[38] Ghittorelli M., Lingstedt L., Romele P., Crăciun N.I., Kovács-Vajna Z.M., Blom P.W.M., Torricelli F., **2018**, *Nature Commun*., 9, 1441.
[39] Bernards D. A., Malliaras G.G., **2007**, *Adv. Funct. Mater.,* 17, 3538-3544.
[40] Lin P., Yan F., Chan H.L.W., **2010**, *ACS Appl. Mater. Interfaces*, *2*, 1637-164.
[41] Bernards D.D., Macaya D.J., Nikolou M., DeFranco J.A., Takamatsua S., Malliaras G.G., **2008**, *J. Mater. Chem.*,18, 116-120.
[42] Rivnay J., Leleux P., Ferro M., Sessolo M., Williamson A., Koutsouras D.A., Khodagholy D., Ramuz M., Strakosas X., Owens R.M., Benar C., Badier J.M., Bernard C., Malliaras G.G., **2015**, *Sci. Adv*, 1:e1400251.
[43] White S.P., Frisbie C.D., Dorfman K.D., **2018**, *ACS Sens*., 3, 395-402.

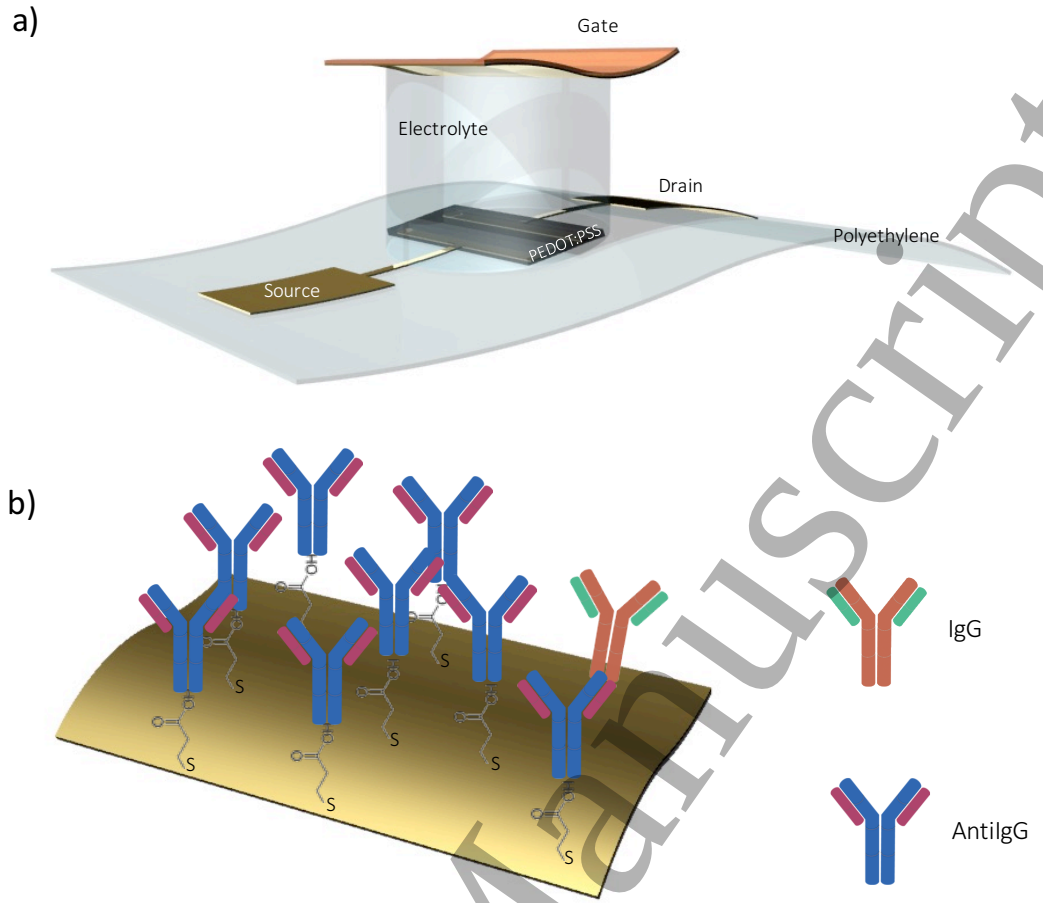


**Figure 1.** (a) Schematic of the OECT device. The source (S) and drain (D) contacts are defined on a flexible and plastic substrate and are covered by printed layer of PEDOT:PSS. A 300 mL of phosphate buffer saline (PBS) is dispensed into a polydimethylsiloxane well covering the organic semiconductor surface. A gold gate electrode is placed over the device at a distance of about 4 mm from the organic semiconductor surface, in contact with the electrolyte. (b) Schematic representation of a self-assembled monolayer (SAM) of the capturing anti-IgGs deposited on the PBS exposed surface of a gold plated Kapton foil.

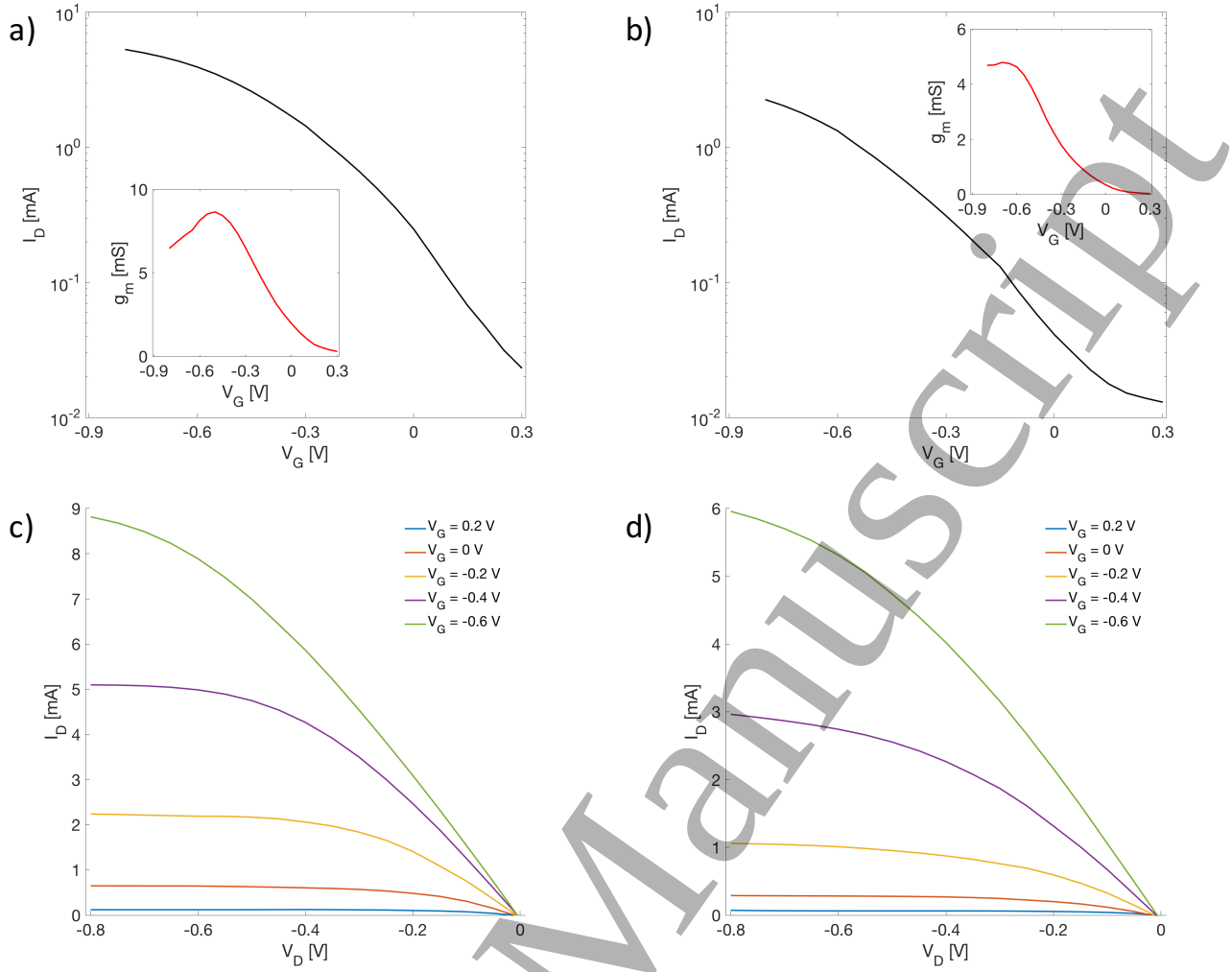


**Figure 2.** Transfer characteristics of an OECT measured with an anti-IgG functionalized gate electrode (a) and a BSA control gate electrode (b), respectively. Insets of (a) and (b) are the corresponding transconductances. Output characteristics measured with anti-IgG gate (c) and BSA gate electrode (d).

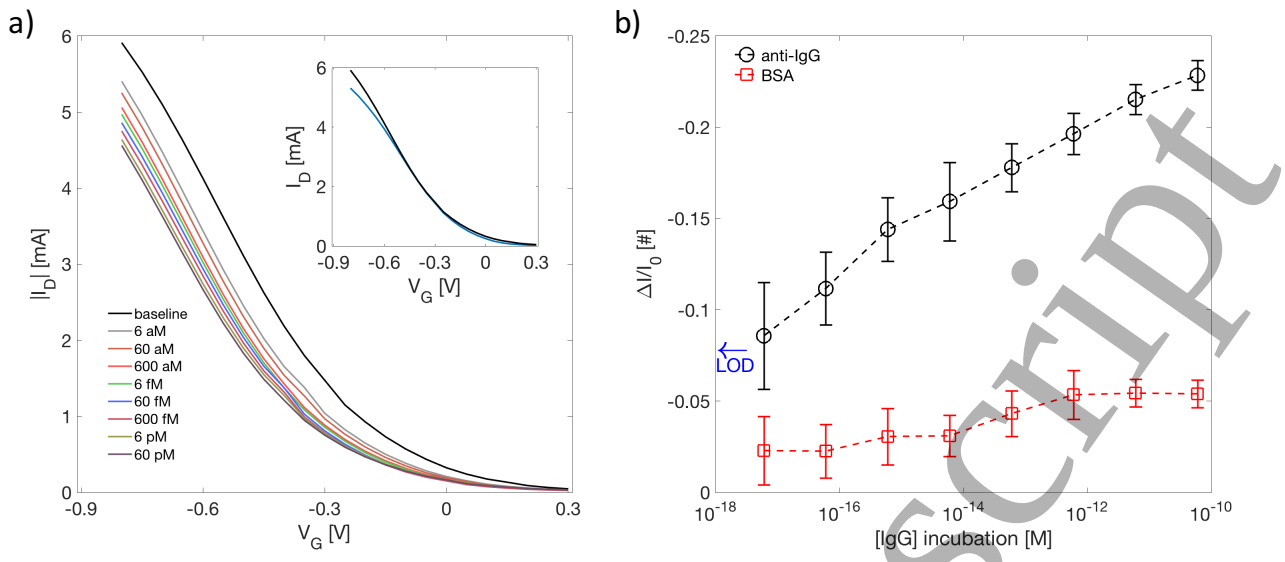


**Figure 3.** (a) Transfer characteristics of an OECT measured with an anti-IgG gate electrode assayed with several concentrations of IgG ranging from 6 aM to 66 pM. The black curve corresponds to the anti-IgG incubated in the bare PBS solution (base-line). Inset: transfer characteristics of an OECT measured before (black line) and after (blue line) the assay. (b) Response of an OECT assayed with different concentrations of IgG using an anti-IgG gate electrode (black curve) or a BSA gate electrode (red curve). The data are based on three replicates and the error bars are taken as the relative standard deviation.

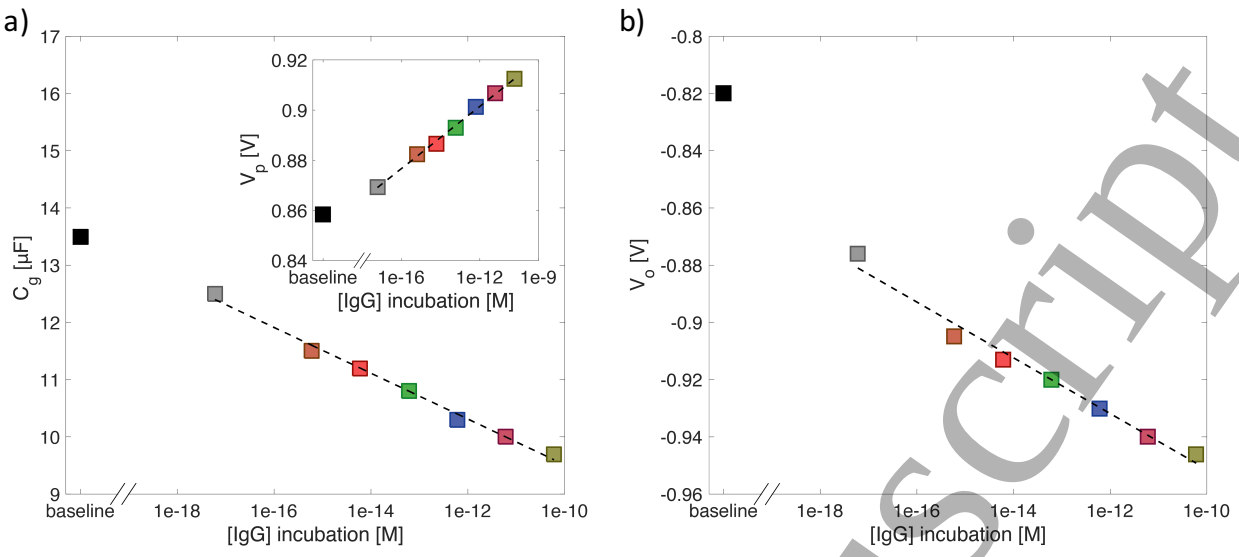


**Figure 4.** (a) Gate capacitance $C_g$ as a function of the IgG concentration. Inset: pinch off voltage $V_p$ as a function of the IgG concentration. $V_p$ is positive because the drain current model (Eqs. 2, 3) describes a p-type OECT. (b) Potential drop at the gate-electrolyte interface $V_o$ as a function of the IgG concentration.